Iranian Journal of Medical Physics
Vol. 9, No. 3, Summer 2012, 203-215
Received: June 20, 2012; Accepted: September 16, 2012

Original Article

A New Method for Characterization of Biological Particles in Microscopic Videos: Hypothesis Testing Based on a Combination of Stochastic Modeling and Graph Theory

Seyed Vahab Shojaedini[1*]

Abstract

Introduction
Studying motility of biological objects is an important parameter in many biomedical processes. Therefore, automated analyzing methods via microscopic videos are becoming an important step in recent researches.
Materials and Methods
In the proposed method of this article, a hypothesis testing function is defined to separate biological particles from artifact and noise in captured video. Then, a decision about each hypothesis is made in the following steps: selecting primary candidates using stochastic modeling, pruning false candidates using graph theory, and confirming remained particles by Kalman filtering.
Results
Performance of the proposed method is evaluated on real videos containing low and high densities of live Listeria particles. The results show that in the first scenario, the proposed and MD algorithms detect 95% and 65% of particles in presence of 2% and 44% false detections, respectively. In the second scenario, the proposed and MD algorithms detect 91% and 55% of particles in presence of 14% and 45% false detections, respectively.
Conclusion
In the first scenario, the proposed algorithm detects and tracks particles typically 30% and 31% better than MD. Moreover, its false detected particles and trajectories are 42% and 27% less than MD. In the second scenario, the proposed method detects and tracks particles typically 36% and 38% better than MD, also its false detected particles and trajectories are 31% and 18% less than MD. Consequently, better characterization of particles in proposed algorithm not only does not lead to extracting more false particles and trajectories but also decreases the rate of false characterized particles and trajectories compared with existing algorithms.

Keywords: Biological Particle, Graph Theory, Hypothesis Testing, Microscopic Video

1-, Iranian Research Organization for Science and Technology, Tehran, Iran
*Corresponding author: Tel & Fax: +98 21 88838350;Email:shojadini@irost.ir

1. Introduction

Motility is a biological term which refers to the capability of moving spontaneously in a biological process which makes use of energy [1]. The motility of small biological objects is an essential part of many biomedical processes and studying it is necessary for the supervision of many living organisms such as motility of rolling leukocytes during the inflammation process [2], motility of gram-negative Escherichia Coli bacteria in meningitis and peritonitis [3], rupturing the cell walls of bacteria by penicillin [4], motility of stem cells in tissue engineering [5], cell motility in embryo development [6], and movement of sperms in male semen which determines the chance of pregnancy [7,8]. New medical imaging technologies allow analyzing the motility of biological particles in vitro and in vivo via microscopic videos [9]. Therefore, accurate characterization and tracking of this motility in microscopic videos are becoming an important step in many biological researches [10] and various methods have been proposed for them. The oldest method is manual characterization and tracking by an expert operator which is the most effort-demanding and time-consuming. Therefore, this method is impractical for many data sets which contain great numbers of biological particles [11]. Therefore, automated methods have become essential for biological particle characterization. Automated characterization methods face several challenges such as: poor image quality, varying particle populations due to mitotic division and particles entering or leaving the field of view, and the possibility of particles touching each other without showing enough contrast in the captured video [12].

Several methods have been proposed for automatic characterization of biological particles. There is one class of methods that characterizes biological particles using their edge and shape information. The close proximity of particles and occlusion are the main limitations of this class of methods [13]. Some methods make use of centroid relocation to characterize biological particles. These methods face many problems because of ignoring a large amount of information about particles such as size, shape, and velocity [14]. Contour-based methods have shown significant potentials for characterization of biological particles but their performance is closely dependent on primary knowledge about the shape and the scale of the particles, which is a considerable limitation for this group of methods [15]. Some researches utilize watershed method to characterize biological particles but this method has some drawbacks such as its sensitivity to noise and its tendency to yield very fragmented results [16]. More sophisticated methods include various types of template matching. These approaches face some challenges such as the need to detect the main template separately by an expert operator, high sensitivity to shape and size of particles, and failing against particle rotations which often occurred in biological particles [17].

In this paper, a new method for characterization of biological particles is introduced which is based on a combination of stochastic modeling and graph theory. In the proposed method, firstly, probable biological particles in each frame are extracted using their stochastic models and considered as “candidates”. In the second step, graph theory based pruning algorithm is applied to candidates during successive frames, which leads to rejection of some false candidates. Finally, a Kalman filter-based algorithm is applied to the remaining candidates to confirm them as biological particles and make their motility trajectories. Unlike the existing methods, the proposed algorithm may use many features of particles such as their history, size, and velocity. Moreover, it does not need primary knowledge about the particles. Furthermore, the proposed method detects particles automatically and is capable of characterizing particles with rotating motility.

The paper is organized as follows. In section II, the proposed algorithm has been introduced including stochastic modeling for candidate selection, graph theory for pruning, and

trajectory making for candidate confirming. In section III, the performance of the proposed method is evaluated in two different scenarios based on real videos recorded from motility of biological particles. In section IV, the experiments results are compared with the corresponding values resulting from existing methods using their effective parameters. Conclusion is presented in the last section of the paper.

2. Materials and Methods

Suppose I is a video stream of biological particles and I_t is a frame of I which is occurred in time slot t. For each pixel of I_t it can be written:

$$I_{tlj} = I_t(l, j) \quad 1 \le l \le L \quad , \quad 1 \le j \le J \quad , \quad 0 \le t \le T \tag{1}$$

In the above equation, I_{tlj} is the amplitude of a pixel in I_t which is located in row and column equal with l and j, respectively. L And J are image sizes and T is the time length of video stream I.

In each time $t_0 + 1$, the dependence of the pixel $I_{(t_0+1)lj}$ to artifact and noise (H_0) or its dependence to a particle (H_1) is determined defining hypothesis testing equation (2):

$$\begin{cases} H_0 : & I_{(t_0+1)lj} = \left| c_{(t_0+1)lj} + n_{(t_0+1)lj} \right| \\ H_1 : & I_{(t_0+1)lj} = \left| s_{(t_0+1)lj} + c_{(t_0+1)lj} + n_{(t_0+1)lj} \right| \end{cases} \tag{2}$$

In the above equation, $s_{(t_0+1)lj}$, $c_{(t_0+1)lj}$ and $n_{(t_0+1)lj}$ show the biological particle, artifact, and noise components in $I_{(t_0+1)lj}$, respectively.

2.1. Candidate Selection

To determine the dependence of $I_{(t_0+1)lj}$ to each of above hypothesis, its history is explained as:

$$\{I_{t_0lj}\} = \{I_{0lj}, I_{1lj}, ..., I_{t_0lj}\} \tag{3}$$

Now $\{I_{t_0lj}\}$ is supposed to be a stochastic process and its distribution function is constructed as:

$$g(I_{t_0lj}) = G(\{I_{t_0lj}\} | \mu_{1t_0lj}, \mu_{2t_0lj}, ..., \mu_{kt_0lj}, ...\mu_{Kt_0lj}) \tag{4}$$

In above equation, μ_{kt_0lj} are K number of distribution parameters of $G(.)$ which must be estimated based on $\{I_{t_0lj}\}$. For brevity μ_{kt_0lj} parameters are shown as:

$$\mu = \{\mu_{1t_0lj}, \mu_{2t_0lj}, ..., \mu_{Kt_0lj}\} \tag{5}$$

Equation (6) can be obtained by combination of (4) and (5) as:

$$G(\{I_{t_0lj}\} | \mu) = G(I_{0lj} | \mu).G(I_{1lj} | \mu)...G(I_{t_0lj} | \mu) \tag{6}$$

The likelihood function $\beta(.)$ is defined as:

$$\beta(\mu | \{I_{t_0lj}\}) = G(\{I_{t_0lj}\} | \mu) = \prod_{t=0}^{t_0} G(I_{tlj} | \mu) \tag{7}$$

Calculating the logarithm of equation (7), it can be written as a sum of probability distribution components as shown in (8):

$$\ln(\beta(\mu | \{I_{t_0lj}\})) = \sum_{t=0}^{t_0} \ln(G(I_{tlj} | \mu)) \tag{8}$$

Now, based on equations (9) $\hat{\beta}$ is defined as the mean of the logarithm form of likelihood function $\beta(.)$ [18].

$$\hat{\beta} = \frac{1}{t_0 + 1} \ln(\beta(\mu | \{I_{t_0lj}\})) \tag{9}$$

Equation (10) shows that μ is estimated as $\hat{\mu}$ by maximization of $\hat{\beta}$ using maximum likelihood estimation [19].

$$\hat{\mu} = \arg\max(\hat{\beta}(\mu | \{I_{t_0lj}\})) \tag{10}$$

Substituting the estimated parameters $\hat{\mu}$ in equation (4), leads to the stochastic model for $I_{(t_0+1)lj}$ based on its history in time period $[0\ t_0]$. Now to determine the belonging of $I_{(t_0+1)lj}$ to biological particle or artifact and noise its dependence probability to the stochastic model (4) is calculated as:

$$Z(I_{(t_0+1)lj}) = P(I_{(t_0+1)lj} | G(\{I_{t_0lj}\} | \hat{\mu})) \tag{11}$$

In which P shows the probability. Now, based on the dependence of each pixel to its history, pseudo-image $I'_{(t_0+1)}$ can be constructed. For this purpose, each pixel of $I_{(t_0+1)}$ which its $Z(I_{(t_0+1)lj})$ is greater than

threshold $\chi_{(t_0+1)lj}$, is primarily associated with artifact or noise and its value considered as 0 in $I'_{(t_0+1)}$. Otherwise, it can be considered as a pixel of a probable biological particle and its value is maintained unchanged in $I'_{(t_0+1)}$. Therefore, the pseudo image $I'_{(t_0+1)}$ contains all pixels which have some chance to be a part of a biological particle as:

$$\begin{cases} I'_{(t_0+1)lj}=0 & Z(I_{(t_0+1)lj})>\chi_{(t_0+1)lj} \\ I'_{(t_0+1)lj}=I_{(t_0+1)lj} & else \end{cases} \quad (12)$$

2.2. Graph Theory-Based Pruning

Based on equation (12), $I'_{(t_0+1)}$ contains pixels of $I_{(t_0+1)}$ which their dependence probabilities to biological particle are greater than their dependence probabilities to artifact and noise. As a result, $I'_{(t_0+1)}$ includes only some candidates and may contain some pixels which do not belong to real biological particles. Therefore, a pruning procedure is applied to I'_{t_0+1} to reject some false candidates. For this purpose, a kind of spatial image processing is used in which the connected candidates in $I'_{(t_0+1)}$ are extracted using a method which has been proposed by Shapiro [20]:

$$\{O_{(t_0+1)}\}=\{O_{(t_0+1)1},...,O_{(t_0+1)w},...,O_{(t_0+1)W}\} \quad (13)$$

In the above equation, $\{O_{(t_0+1)}\}$ is the set of connected candidates extracted from I'_{t_0+1}, $O_{(t_0+1)w}$ is the candidate w from this set and W is the number of candidates in I'_{t_0+1}. Similar to the above set, the string $\lambda_{(t_0+1)}$ is defined as shown in equation (14).

$$\{\lambda_{(t_0+1)}\}=\{\lambda_{(t_0+1)1},...,\lambda_{(t_0+1)w},...,\lambda_{(t_0+1)W}\} \quad (14)$$

In the equation above, $\lambda_{(t_0+1)w}$ shows number of pixels belonging to candidate $O_{(t_0+1)w}$. In the next step, the members of $\{O_{(t_0+1)}\}$ are ordered due to the number of pixels belonging to each of them. Then, based on equation (15) and (16), the new set of candidates $\{O'_{(t_0+1)}\}$ is constructed using the F superior members of $\{O_{(t_0+1)}\}$ which numbers of their pixels are greater than α.

$$\{O'_{(t_0+1)}\}=\{O'_{(t_0+1)1},...,O'_{(t_0+1)f},...,O'_{(t_0+1)F}\} \quad (15)$$

$$f=1,2,...,F$$

$$O'_{(t_0+1)f}=O_{(t_0+1)w} \ , \ \lambda_{(t_0+1)w}>\alpha \quad (16)$$

In above equations, $O'_{(t_0+1)f}$ shows the f th candidate for biological particle in frame t_0+1 of video stream I. The algorithm which was mentioned during equations (1)-(16) is also applied to frame t_0+2 of video stream, e.g., I_{t_0+2}, and similar to equations (15) and (16), F' candidates are extracted in this frame as:

$$\{O'_{t_0+2}\}=\{O'_{(t_0+2)1},...,O'_{(t_0+2)f'},...,O'_{(t_0+2)F'}\} \quad (17)$$

$$f'=1,2,...,F'$$

To complete the pruning of false candidates, it is necessary to assign a member of $\{O'_{(t_0+1)}\}$ -like $O'_{(t_0+1)f}$- to a member of $\{O'_{t_0+2}\}$ -like $O'_{(t_0+2)f'}$- in such a way that they can be considered as a unit biological particle in two frames t_0+1 and t_0+2. For this purpose, the following steps are done:

Feature vectors for all members of $\{O'_{(t_0+1)}\}$ and $\{O'_{(t_0+2)}\}$ are extracted containing centroid coordinates, velocity in image dimensions, size, and size rate. For instance, $X_{(t_0+1)f}$ and $X_{(t_0+2)f'}$ are feature vectors of $O'_{(t_0+1)f}$ and $O'_{(t_0+2)f'}$, respectively. Therefore, $\{X_{(t_0+1)}\}$ and $\{X_{(t_0+2)}\}$ are feature spaces for $\{O'_{(t_0+1)}\}$ and $\{O'_{(t_0+2)}\}$.

Each matched pair $X_{(t_0+1)f}$ and $X_{(t_0+2)f'}$ in $\{X_{(t_0+1)}\}$ and $\{X_{(t_0+2)}\}$ indicates a unique biological particle. To evaluate the association, the Euclidian distance is calculated between all $\{X_{(t_0+1)}\}$ and $\{X_{(t_0+2)}\}$ members that leads to a distance matrix illustrated as:

$$D_{t_0+1,t_0+2}=\begin{bmatrix} d_{11}\,d_{12}\ \ldots d_{1f}\ldots d_{1q}\ldots d_{1F} \\ d_{21}\,d_{22}\ \ldots d_{2f}\ldots d_{2q}\ldots d_{2F} \\ \vdots \\ d_{f'1}\,d_{f'2}\ \ldots d_{f'f}\ldots d_{f'q}\ldots d_{f'F} \\ \vdots \\ d_{q'1}\,d_{q'2}\ \ldots d_{q'f}\ldots d_{q'q}\ldots d_{q'F} \\ \vdots \\ d_{F'1}\,d_{F'2}\ \ldots d_{F'f}\ldots d_{F'q}\ldots d_{F'F} \end{bmatrix} \quad (18)$$

In the above matrix, $q=1,2,...,F$ and $q'=1,2,...,F'$ have same definitions as f, f', and $d_{f'f}=\left\|X_{(t_0+2)f'}-X_{(t_0+1)f}\right\|$ which is the Euclidian distance.

The vector $X_{(t_0+2)f'}$ is selected from vector space $\{X_{(t_0+2)}\}$ and is compared with vector $X_{(t_0+1)f}$ from vector space $\{X_{(t_0+1)}\}$. In this paper, a kind of graph matching algorithms is used for this comparison as follows [21]:

If no member of $\{X_{(t_0+2)}\}$ was matched with $X_{(t_0+1)f}$, then $X_{(t_0+1)f}$ is selected as matched pair of $X_{(t_0+2)f'}$ and their dependence is shown by putting 1 in $f'f$ element of association matrix constructed in frame t_0+2 which is shown as $[M]_{(t_0+2)F'F}$.

If $X_{(t_0+1)f}$ had a matched pair in $\{X_{(t_0+2)}\}$ like $X_{(t_0+2)q'}$ then and if $d_{f'f}<d_{q'f}$, it means that $X_{(t_0+2)f'}$ is closer to $X_{(t_0+1)f}$ than $X_{(t_0+2)q'}$ and consequently matching of $X_{(t_0+1)f}$ and $X_{(t_0+2)q'}$ is neglected and $X_{(t_0+1)f}$ is matched to $X_{(t_0+2)f'}$ by putting 0 and 1 in $q'f$ and $f'f$ indices of $[M]_{(t_0+2)F'F}$, respectively.

If $X_{(t_0+1)f}$ had an matched pair in $\{X_{t_0+2}\}$ like $X_{(t_0+2)q'}$ but $d_{f'f}\geq d_{q'f}$, it means that $X_{(t_0+2)q'}$ is closer to $X_{(t_0+1)f}$ than $X_{(t_0+2)f'}$, then $q'f$ and $f'f$ indices of $[M]_{(t_0+2)F'F}$ remain unchanged as 1 and 0, respectively.

The above (a), (b), and (c) steps are applied to all $\{X_{(t_0+2)}\}$ and $\{X_{(t_0+1)}\}$ feature vectors and the final association matrix $[M]_{(t_0+2)F'F}$ is obtained. Each pair of vectors in $\{X_{(t_0+2)}\}$ and $\{X_{(t_0+1)}\}$ which their related member in $[M]_{(t_0+2)F'F}$ is indicated by 1 shows a matched pair and specify a characterized biological particle. Flowchart of pruning procedure has been shown in Figure 1.

2.3. Confirming Particles by Obtaining Their Motility Trajectories

In this stage, a Kaman-based algorithm is applied to each remained candidate to confirm it by obtaining a meaningful motility trajectory. Suppose that

$$\theta_{t_0+2}=\{X_{(t_0+2)\eta},\eta=1,2,...,B\}$$
$$X_{(t_0+2)\eta}=X_{(t_0+2)f}\ ,\ M_{(t_0+2)}(f',f)=1 \quad (19)$$

Which θ_{t_0+2} contains B remained candidates in frame t_0+2 after the mentioned pruning in II.2. Similarly, θ_{t_0+3} contains B' remained candidates in t_0+3.

$$\theta_{t_0+3}=\{X_{(t_0+3)\eta'},\eta'=1,2,...,B'\} \quad (20)$$

Therefore, for each member of θ_{t_0+2} such as $X_{(t_0+2)\eta}$ confirming and finding motility trajectory is defined as finding unique $X_{(t_0+3)\eta'}$ in such a way that it can be considered as the future of $X_{(t_0+2)\eta}$ in frame t_0+3. In this paper, a Kaman filter like ψ_η has been used for this purpose. This procedure for each ψ_η is as follows:

For each $X_{(t_0+3)\eta'}$, if it satisfies ψ_η then $X_{(t_0+3)\eta'}$ is indicated as the future of ψ_η and the filter is updated. If the number of updates exceeds a threshold γ then its associated candidate is considered as "*Confirmed*".

If no member of θ_{t_0+3} satisfies ψ_η, then the ψ_η in frame t_0+3 is considered as lost and its estimation is accomplished using its history temporarily. Moreover, if the loosed frames for a candidate are more than a threshold, then it is considered as "*False*" and it will be rejected.

Those members of θ_{t_0+3} who hasn't been associated to any ψ_η, are fed to pruning algorithm II.2, to find new candidates.

Finally, combination of (2) and (19) with confirming procedure leads to equation (21) which determines the state of each pixel of the main video in a sample time such as t_0+1.

$$\begin{cases} reject(H_0) \equiv H_1 : \ I_{(t_0+1)lj} \in O'_{(t_0+1)f}, \\ X_{(t_0+1)f} = (X_{(t_0+1)\eta} \in \theta_{t_0+1}), \\ length(\psi_\eta) > \gamma \quad \equiv \\ I_{(t_0+1)lj} = \left| s_{(t_0+1)lj} + c_{(t_0+1)lj} + n_{(t_0+1)lj} \right| \\ Do\ not\ reject(H_0): \quad Otherwise \end{cases} \tag{21}$$

Note that concluding "Do not reject H_0" doesn't necessarily mean that H_0 is true, it only shows that there is no sufficient evidence against H_0 in favor of H_1 [22] and therefore the pixel cannot be considered as a part of biological particle in current time slot.

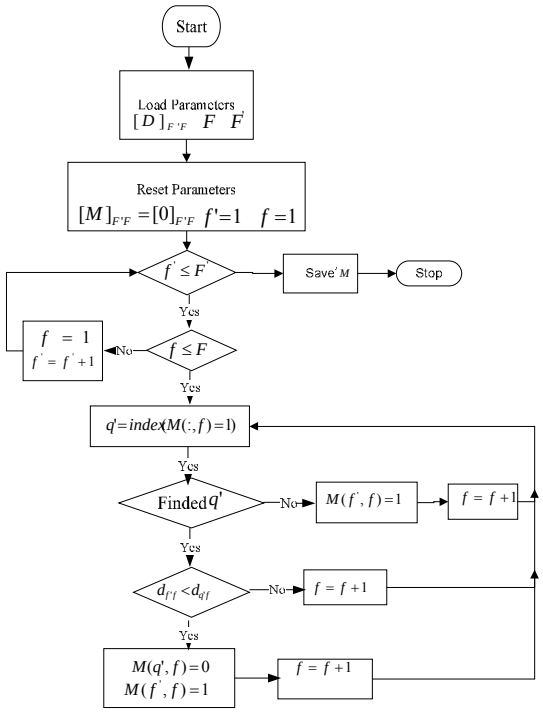

Figure 1. Pruning procedure.

3. Results

The proposed algorithm was applied to real data. The data set was various videos which had been obtained from microscopy of live Listeria activity. Listeria is a kind of Gram-positive bacilli which exists in contaminated meat and vegetables and affects the human immune system which leads to the fatal disease, "Listeriosis" [23]. The videos were captured by an Orca ER Digital CCD camera mounted on a Nikon invert microscope using a 40× zoom lens. Variations in optical filtering, shutter time, and light exposure led to variations of the captured videos in contrast, intensity, and apparent proximity.

The proposed method was implemented using Matlab 2009. Additionally, algorithm of morphological detection (MD) of biological particles [24] was implemented to be compared with the proposed algorithm. Tests were carried out on different scenarios which in one of them the test specimens contained low density particles, so simple motions were seen in captured videos and in another one specimens contained high density particles, so complex and close motions appeared in captured videos. Specifications of both scenarios have been shown in Table 1. The captured videos were first processed using manual characterization to obtain a ground-truth characterization to compare the automatic methods with. Then, characterized particles were obtained by applying the proposed and MD algorithms and the performance of each algorithm was determined by comparing its results with manual characterization results.

3.1. First scenario

In the first scenario, the captured video had been obtained from specimens which contained low density live Listeria particles ($<10\,CFU/ml$ [1]concentration) which had single motion trajectories.

Figures (2) and (3) show obtained results in four different frames (15, 20, 25, and 30) of this scenario utilizing the proposed and MD methods, respectively. For instance, in Figure 2-a result of frame 15 shows that the proposed method has extracted 5 particles from 5 original particles (marked as 1-5) with no false particle. Moreover, Figure 2-b shows that the proposed method has extracted all of 5 particles of frame 15 with no false particle again in frame 20. However, Figure 3 shows that MD method has had weaker results than the proposed method.

[1] Colony Forming Unit Per milliliter

Table 1. Specifications of test scenarios.

Specification	Value	Specification	Value
sizes of particles	Min: 12 pixels Max: 70 pixels	Number of captured frames	Scenario1: 117 Scenario 2: 150
Frame size	240*320 pixels	Min and Max speed of particles	Scenario1: 0.2-2.5 pixels per frame * Scenario 2: 0.5-6 pixels per frame
Video frame rate	25 fps	Average contrast	18%

*Note that 0.2 pixel per frame means that the movement has been averagely one pixel per 5 frames

It is obvious in Figure 3-a, that MD method has extracted two particles correctly (marked as 1 and 5) on the same frame as Figure 2-a, so it has missed 3 original particles. Moreover, it has extracted 4 false particles (marked as 2, 3, 4, and 6). The results which have been shown in Figure 3-b indicates that in frame 20, MD has extracted 3 particles correctly (marked as 1, 5, and 7) and has missed 2 particles. Moreover, MD has extracted 4 false particles (marked as 2, 3, 4, and 6). Similar results which have been obtained from frames 25 and 30 of Figures 2 and 3 still show the better performance of the proposed method compared with MD.

3.2. Second scenario

In this scenario, the video stream was captured from specimens containing high density ($>10\,CFU/ml$ concentration) and high speed live Listeria particles. These particles had complex trajectories which caused some limitations in video such as: dividing particles, exiting of some particles from the region of interest, particle apoptosis, and particles with close distances.

Figures 4 and 5 show results which have been obtained in four different frames (15, 20, 25, and 30) of this scenario utilizing the proposed and MD methods, respectively.

For example, in Figure 4-a, result of frame 15 shows that the proposed method has extracted 16 particles from 17 original particles (only one missed particle) with two false particles (marked as 2 and 11). Moreover, in Figure 4-b, result from frame 20 shows that the proposed method has extracted all extracted particles of frame 15 with the same labels. Moreover, it has again extracted two false particles.

In the same scenario situation, MD method has still had weaker results than the proposed method. This fact has been shown in Figure 5. In frame 15 (e.g., 5-a), it is obvious that MD method has extracted 13 particles correctly (4 missed original particles) and 6 false particles (marked as 3, 4, 7, 8, 10, and 12). Moreover, result of frame 20 (e.g., 5-b) shows that MD has extracted 14 particles correctly (3 missed original particles) and 4 false particles (marked as 8, 10, 12, and 14). Similar results which have been obtained from frames 25 and 30 still show the better performance of the proposed method compared with MD.

4. Discussion

Real data which had been obtained from microscopy of live Listeria activity were analyzed. The proposed and MD methods were applied to the data and the results were compared with manual results using the following parameters:

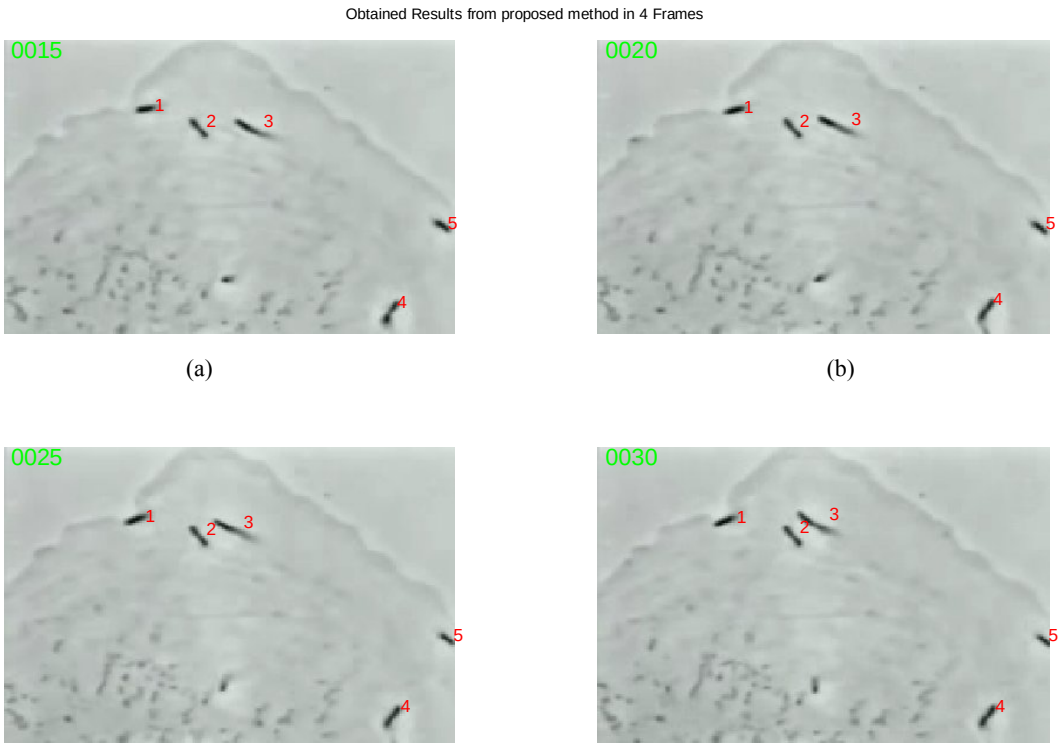

(a) (b)

(c) (d)

Figure 2. Extracted particles using our algorithm in frames (a) 15, (b) 20, (c) 25, and (d) 30 for test specimen containing low density- simple movement live Listeria particles (first scenario).

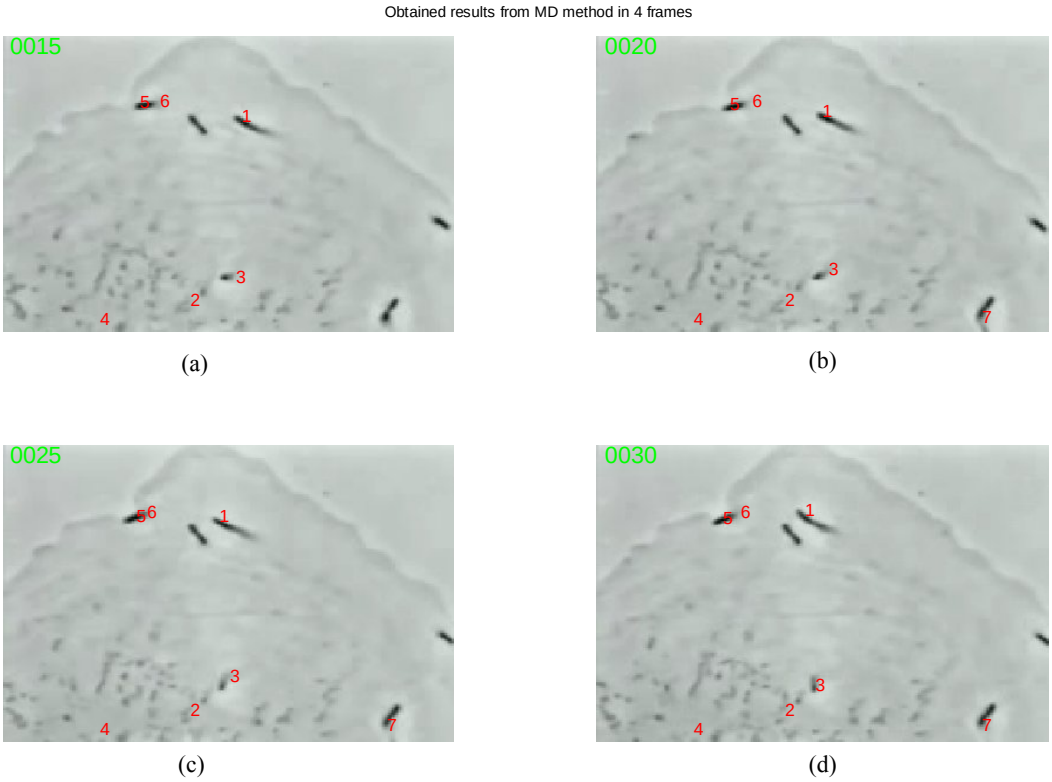

(a) (b)

(c) (d)

Figure 3. Extracted particles using MD algorithm in frames (a) 15, (b) 20, (c) 25, and (d) 30 for a test specimen containing low density- simple movement live Listeria particles (first scenario).

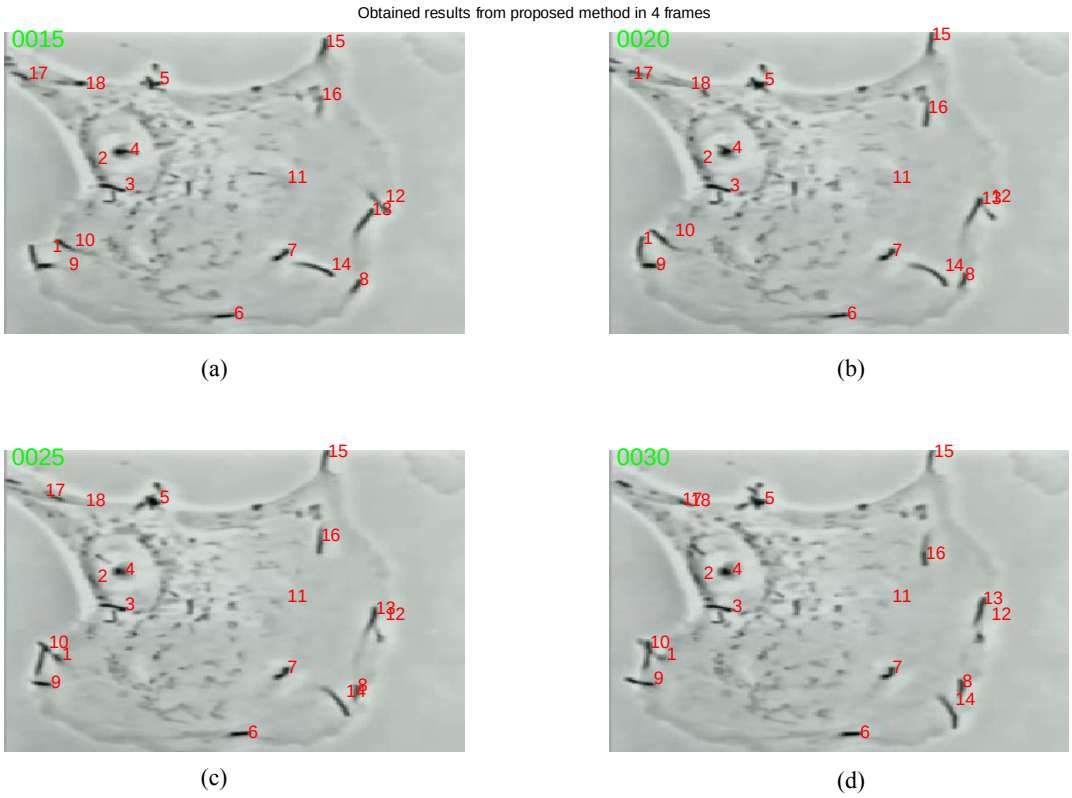

Figure 4. Extracted particles using our algorithm in frames (a) 15, (b) 20, (c) 25, and (d) 30 for a specimen containing high density- complex movement live Listeria particles (second scenario).

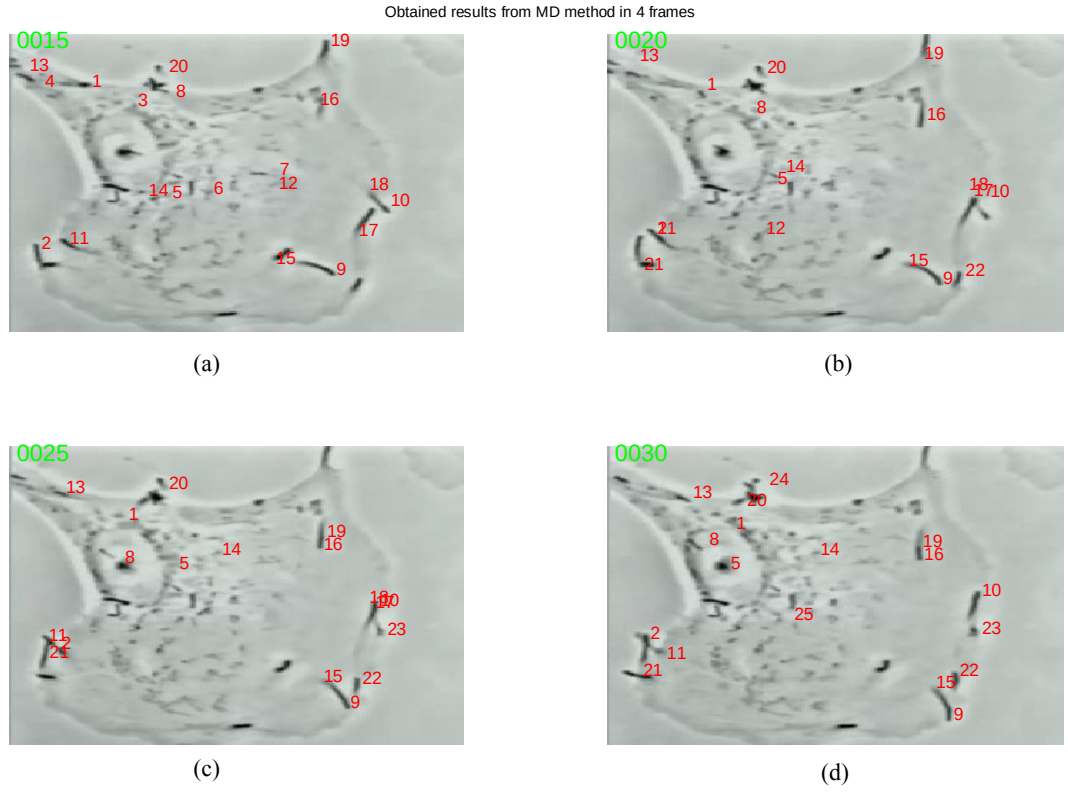

Figure 5. Extracted particles using MD algorithm in frames (a) 15, (b) 20, (c) 25, and (d) 30 for a specimen containing high density-complex movement live Listeria particles (second scenario).

4.1. Detection Rate

To estimate this parameter in each frame, the number of missed particles was determined, then the average for all the frames was calculated and finally it was divided to the total number of particles as:

$$Detection-Rate= \left(1-\frac{\sum_{k=1}^{total\ frames} Missed\ particles\ in\ frame\ k}{total\ frames \times number\ of\ particles}\right)*100 \quad (22)$$

4.2. False Detection Rate

This parameter was calculated similar to equation (22) as:

$$False-Detection-Rate \frac{\sum_{k=1}^{total\ frames} false\ particles\ in\ frame\ k}{total\ frames \times number\ of\ particles}*100 \quad (23)$$

Using the mentioned parameters, ROC curves were obtained for both proposed and MD methods which show changes of detection rate versus false detection rate. ROC curves obtained in the first and second scenarios have been shown in Figures 6 and 7, respectively. These figures show clearly the superiority of the proposed method compared with MD in both of scenarios.

For instance, as shown in Figure 6, the proposed and MD algorithms achieved detection rates of 95% and 65% at the false detection rates of 2% and 44% in the first scenario. In the same manner, the obtained ROC curves for the second scenario (Figure 7) show detection rates of 91% and 55% at false detection rates of 14% and 45% for the proposed and MD algorithms, respectively.

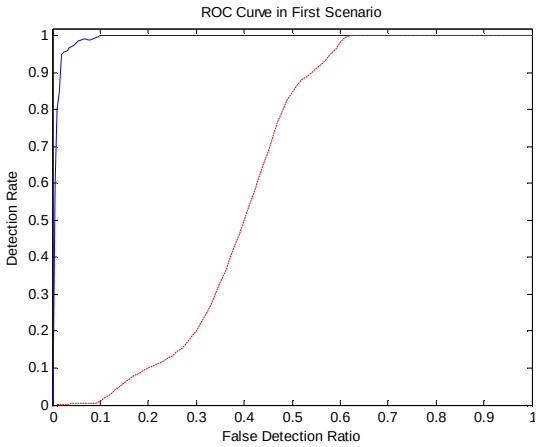

Figure 6. ROC curves obtained in the first scenario for proposed (solid-line) and MD (dashed-line) algorithms.

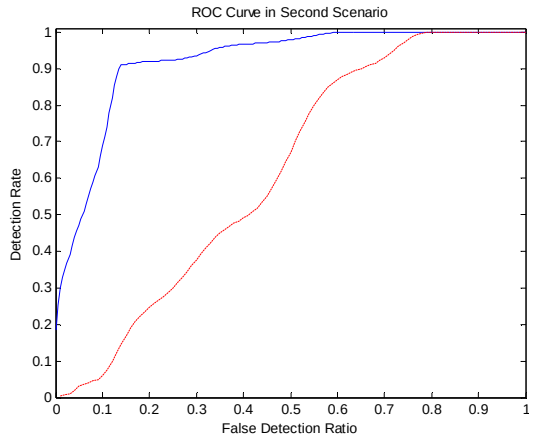

Figure 7. ROC curves obtained in the second scenario for proposed (solid-line) and MD (dashed-line) algorithms.

Based on these results, it can be concluded that typically for each arbitrary particle, its detection probability is considerably (30%, 36% in first and second scenarios, respectively) higher than MD method by using proposed algorithm. Moreover, false detected particles in the proposed method are typically 42% and 31% less than MD in the two scenarios.

4.3. Track categories

In captured videos, all the live Listeria particles may not be tracked because of reasons which were explained in part 3.2. Based on those limitations, constructed trajectories of particle movements were divided into three categories: "*Full Trajectory*" for the particle correctly tracked along the entire video, "*Partial*

Trajectory" for the particle correctly tracked only for a portion of the video, and "*Non-Trajectory*" for the particle incorrectly tracked.

Table 2 shows superiority of the proposed algorithm compared with MD in tracking as well as its superiority in detection. It has been shown that the proposed algorithm extracted full trajectories 31% and 38% better than MD in first and second scenarios, respectively. Moreover, it can be shown that the proposed algorithm has not extracted any non-trajectory in the first scenario whereas the percentage of extracted non-trajectories by MD has been 27% in this scenario. Also, in the second scenario MD has extracted non-trajectories 18% more than the proposed method.

The superior performance of our proposed algorithm is due to its different treatment of random changes in each frame. Specifically, it should be noted that the contents of the captured video from biological particles change randomly during successive frames as mentioned before. Existing methods characterize particles using conventional spatial processing only. On the contrary, our method treats the random changes of pixels of captured frames as a stochastic process. Firstly, it extracts candidates for biological particles by exploiting the aforementioned stochastic models and then confirms them utilizing a combination of graph theory and spatial processing. Such stochastic modeling which is more compatible with the nature of these images can select more correct particles and reject more false particles compared with existing alternatives which do not consider such stochastic nature and models. This intuition is further corroborated by the obtained results mentioned before.

Finally, it is notable that the performances of both algorithms have been decreased in the second scenario compared with their performances in the first scenario. Table 2 shows that in the second scenario, full trajectories have been decreased 6% and 13% by using the proposed and MD methods, respectively.

Table 2. Comparing performance of algorithms in different scenarios.

	Parameter	First Scenario		Second Scenario	
		Our	MD	Our	MD
Detect	Detection Rate	95%	65%	91%	55%
Detect	False-Detection-Rate	2%	44%	14%	45%
Track	Full Trajectory	100%	69%	94%	56%
Track	Partial Trajectory	0%	16%	6%	15%
Track	None Trajectory	0%	27%	12%	30%

In the same manner, non-trajectories of the proposed and MD methods increased 12% and 3% compared with their values in the first scenario. This performance degradation may be explained by the presence of higher concentration of live Listeria particles and their more complex movement in the second scenario compared with the first scenario.

5. Conclusion

In this paper, a new method was introduced for characterization of live Listeria particles in microscopic videos. In the proposed method, firstly, some probable particles were indicated as "candidates" by modeling their history as a stochastic process. Such a stochastic modeling makes the proposed algorithm different from existing methods and allows us to consider changes of captured video during successive frames. In the second step, the graph theory was utilized to reject some candidates that had not constructed a meaningful string in successive frames. In the final step, biological particles were characterized from those remaining candidates who had made motility trajectories for a required period of time.

To evaluate the performance of the proposed algorithm, two scenarios were carried out based on real videos containing live Listeria particles. The first scenario belonged to specimens with low density of particles, so simple motions would appear in captured videos. The second scenario

dealt with specimens with high density of particles, so complex and close motions were recorded in captured videos. In both scenarios, the performance of the proposed algorithm was compared with MD method using their detection rate, false detection rate, full trajectories, partial trajectories, and non-trajectories. Results showed higher performance of the proposed algorithm in characterization of biological particles compared with MD method. By exploiting the obtained ROC curves, it was shown that in the first scenario, the proposed algorithm has characterized typically 95% of particles and 100% of full-trajectories. The above results have been 30% and 31% better than those which had been obtained using MD. Moreover, for the proposed algorithm, false detected particles and non-trajectories have been 42% and 27% better than those obtained by the MD algorithm. In the second scenario, biological particles had higher concentrations and their movements were more complex which led to degradation of results compared with the former scenario. However, it was shown that in this scenario the proposed method characterized particles 36% and 38% better than MD using detection rate and full-trajectory parameters. Furthermore, for the proposed algorithm, the rate of the false detected particles and non-trajectories have been 31% and 18% better than MD. Therefore, it shows that better characterization of particles and trajectories by proposed algorithm not only has not led to the extraction of more false particles and non-trajectories, but also has decreased their erroneous values. Consequently, it can be concluded that the proposed method may be used as a suitable choice for characterization of biological particles and their motility trajectories.

Acknowledgements

The authors are thankful to Dr Mohamad Kalantari for sincere discussions and editing parts of this article.

References

1. Lenz P. Cell Motility: Springer; 2008.
2. Acton S, Ley K. Tracking leukocytes from in vivo video microscopy using morphological anisotropic diffusion. Proc Int Conf Image Proc. 2001 Oct 2: 300-3.
3. Xie J, Khan S, Shah M. Automatic tracking of Escherichia coli in phase-contrast microscopy video. IEEE Trans Biomed Eng. 2009 Feb;56(2):390-9.
4. Milović NM, Wang J, Lewis K, Klibanov AM. Immobilized N-alkylated polyethylenimine avidly kills bacteria by rupturing cell membranes with no resistance developed. Biotechnol Bioeng. 2005 Jun 20;90(6):715-22.
5. Min L, Roy-Chowdhury AK, Venugopala Reddy G, editors. Robust estimation of stem cell lineages using local graph matching. Computer Vision and Pattern Recognition Workshops, 2009 CVPR Workshops 2009 IEEE Computer Society Conference on; 2009 20-25 June 2009.
6. Paduano V, Sepe L, Cantarella C, Sansone C, Paolella G, Ceccarelli M, editors. Time-lapse phase-contrast microscopy fibroblast automated tracking. Imaging Systems and Techniques (IST), 2010 IEEE International Conference on; 2010 1-2 July 2010.
7. Zheng Li X, Wang Zhi Y, editors. The sperm video segmentation based on dynamic threshold. Machine Learning and Cybernetics (ICMLC), 2010 International Conference on; 2010 11-14 July 2010.

8. Wenzhong Y, Shuqun S. Automatic Chromosome Counting Algorithm Based on Mathematical Morphology. Journal of Data Acquisition & Processing. 2008;23(9):1004-9037.
9. Wu Q, Merchant F, Castleman KR. Microscope Image Processing: Elsevier/Academic Press; 2008.
10. Goobic AP, Welser ME, Acton ST, Ley K, editors. Biomedical application of target tracking in clutter. Signals, Systems and Computers, 2001 Conference Record of the Thirty-Fifth Asilomar Conference on; 2001 4-7 Nov. 2001.
11. Menkveld R, Kruger T. Evaluation of sperm morphology by light microscopy, Assisted Reproduction. 2nd Edition, Partheon Publishing Group, 1996.
12. Chowdhury AS, Chatterjee R, Ghosh M, Ray N, editors. Cell Tracking in Video Microscopy Using Bipartite Graph Matching. Pattern Recognition (ICPR), 2010 20th International Conference on; 2010 23-26 Aug. 2010.
13. Wählby C, SINTORN IM, Erlandsson F, Borgefors G, Bengtsson E. Combining intensity, edge and shape information for 2D and 3D segmentation of cell nuclei in tissue sections. Journal of Microscopy. 2004;215(1):67-76.
14. Schütz GJ, Schindler H, Schmidt T. Single-molecule microscopy on model membranes reveals anomalous diffusion. Biophys J. 1997 Aug;73(2):1073-80.
15. Xinyu L, Yifei W, Yu S. Cell Contour Tracking and Data Synchronization for Real-Time, High-Accuracy Micropipette Aspiration. Automation Science and Engineering, IEEE Transactions on. 2009;6(3):536-43.
16. Xiaodong Y, Houqiang L, Xiaobo Z, Wong S, editors. Automated segmentation and tracking of cells in time-lapse microscopy using watershed and mean shift. Intelligent Signal Processing and Communication Systems, 2005 ISPACS 2005 Proceedings of 2005 International Symposium on; 2005 13-16 Dec. 2005.
17. Bhaskar H, Kingsland RL, Singh S, Welsh G, Tavare J, editors. Multiple Cell-Particle Tracking Based on Multi-Resolution Block-Matching using Genetic Algorithm. Advances in Medical, Signal and Information Processing, 2006 MEDSIP 2006 IET 3rd International Conference On; 2006 17-19 July 2006.
18. DeGroot MH. Probability and statistics: Addison-Wesley Pub. Co.; 1986.
19. Myung IJ. Tutorial on maximum likelihood estimation. Journal of Mathematical Psychology. 2003;47(1):90-100.
20. Shapiro, L. and Haralick, R. Computer and Robot Vision., Addison-Wesley Pub. Co.; 1992, pp. 28-48.
21. Gusfield D, Irving RW. The Stable Marriage Problem: Structure and Algorithms: MIT Press; 1989.
22. Kay SM. Fundamentals of Statistical Signal Processing, Volume 2: Detection Theory. Prentice Hall Signal Processing Series; 1998.
23. Ryser ET, Marth EH. Listeria, listeriosis, and food safety: CRC; 2007.
24. Sertel O, Kong J, Lozanski G, Catalyurek U, Saltz J. Computerized microscopic image analysis of follicular lymphoma. Proceedings of SPIE. 2008;6915:1-11.